



A novel heteropolysaccharide isolated from custard apple pulp and its immunomodulatory activity in mouse macrophages and dendritic cells

Chunhua Huang^{a,1}, Wensong Tu^{b,1}, Man Zhang^{c,1}, Dan Peng^a, Zhongyi Guo^a, Weijuan Huang^a, Jianhua Zhu^b, Rongmin Yu^{b,c,*}, Liyan Song^{a,**}, Yurong Wang^{d,***}

^a Department of Pharmacology, College of Pharmacy, Jinan University, 601 Huangpu Avenue West, Guangzhou 510632, China

^b Biotechnological Institute of Chinese Materia Medica, Jinan University, 601 Huangpu Avenue West, Guangzhou 510632, China

^c Department of Natural Product Chemistry, College of Pharmacy, Jinan University, 601 Huangpu Avenue West, Guangzhou 510632, China

^d Department of Chinese Medicine, Guangzhou First People's Hospital, School of Medicine, South China University of Technology, Guangzhou 510641, China

ARTICLE INFO

Keywords:

Custard apple pulp
Heteropolysaccharide
Immunomodulation
Antigen presenting cells
MAPKs
NF-κB

ABSTRACT

In this study, a novel heteropolysaccharide (ASPA80-1) with an average molecular weight of 5.48×10^4 Da was isolated and structurally elucidated from custard apple pulp (*Annona squamosa*) through DEAE-cellulose, Sephadex G-100 and Sephacryl S-300 HR chromatography and spectral analysis. ASPA80-1 is a water-soluble polysaccharide and it is a polymer consisting of predominant amounts of (1 → 3)-linked-L-arabinose (Ara) residues, small amounts of (1 → 6)-linked-D-galactose (Gal), (1 → 3,5)-linked-L-arabinose (Ara) residues and terminal linked-L-arabinose (Ara) residues, trace amount of (1 → 4)-linked-D-glucose (Glc) residues and (1 → 2)-linked-L-rhamnose (Rham) residues. ASPA80-1 showed significant effect on antigen-presenting cells (APCs) activation. On the one hand, ASPA80-1 activated RAW264.7 macrophage cells by inducing morphology change, enhancing phagocytic ability, increasing nitric oxide (NO) secretion and promoting expression of major histocompatibility complex class II (MHC II) and cluster of differentiation 86 (CD 86). On the other hand, ASPA80-1 promoted the maturation of dendritic cells (DCs) by inducing longer dendrites, decreasing phagocytic ability and increasing MHC II and CD86 expression. Furthermore, mitogen-activated protein kinases (MAPKs) and nuclear factor kappa B (NF-κB) signaling pathways were activated after the intervention of ASPA80-1 on RAW264.7 cells or DCs. Thus, the novel heteropolysaccharide ASPA80-1 has the potential to be used as an immunoenhancing component in functional foods.

* Corresponding author. Biotechnological Institute of Chinese Materia Medica, Jinan University, 601 Huangpu Avenue West, Guangzhou 510632, China

** Corresponding author. Department of Pharmacology, College of Pharmacy, Jinan University, 601 Huangpu Avenue West, Guangzhou 510632, China

*** Corresponding author. Department of Chinese Medicine, Guangzhou First People's Hospital, School of Medicine, South China University of Technology, Guangzhou 510641, China

E-mail addresses: tyrm@jnu.edu.cn (R. Yu), tsly@jnu.edu.cn (L. Song), wangyurong789@163.com (Y. Wang).

¹ The authors contribute to this work equally

<https://doi.org/10.1016/j.heliyon.2023.e18521>

Received 11 January 2023; Received in revised form 8 July 2023; Accepted 19 July 2023

Available online 23 July 2023

2405-8440/© 2023 The Authors. Published by Elsevier Ltd. This is an open access article under the CC BY-NC-ND license (<http://creativecommons.org/licenses/by-nc-nd/4.0/>).

1. Introduction

Polysaccharides consisting of sugar units by glycosidic linkages belong to macromolecular polymers. Polysaccharides are beneficial to health. Numerous studies have reported that polysaccharides possess immunoregulatory, hypoglycemic, neuroprotective, anti-cancer and anti-inflammatory activities [1–5]. Among them, immunoregulatory effects are considered as the primary activity. Nowadays, several polysaccharides have been applied clinically in treating diseases, such as lentinan, schizophyllan, and maitake D-fraction [4]. In addition, it is reported that polysaccharides not only possess low-toxic, non-antigenic, and no obvious side effects but also have the advantages of good water solubility, stable quality and a wide range of sources [6]. Thus, focusing on discovering high efficient and low toxic polysaccharides from plants would be an excellent way to develop immunoregulators.

Custard apple (*Annona squamosa* L.) is a green cone-shaped fruit with leathery skin and creamy, sweet flesh belonging to the family of *Annonaceae*. It is widely distributed in the tropical areas of China, Thailand, India and South America [7]. Its beneficial health effects have been documented in the oldest Chinese pharmacopoeia and it is known for its heat-clearing and detoxicating functions. The multiple chemical components isolated from the leaves, pulp, peel and seeds of the custard apple have been reported to possess potent beneficial properties including antitumor, antioxidant, and antidiabetic activities [8–13]. Few studies have investigated the chemical structure and immunomodulatory activity of the polysaccharides purified from the ripe custard apple. Therefore, it would be valuable to study the custard apple's polysaccharide and its immunoregulatory effect.

DCs is one of the most specialized APCs, which can uptake, process, and present antigens to naïve T cells [14]. It is possible for immature DCs to differentiate into mature DCs when stimulated. Mature DCs are characterized by longer dendrites, higher levels of MHC and co-stimulatory molecules (CD86 and CD80) as well as weak phagocytic ability [15]. MHC molecules are capable of binding with antigens processed by DCs, so that antigens can be presented to T cells more efficiently. DCs can provide essential secondary signals to T cells to initiate immune response via co-stimulatory molecules [16]. DCs are generally few in number and impaired in function especially when distributed in the tumor microenvironment, which may contribute to disappointing results in the DC-induced immune response [17,18]. Therefore, it is essential to promote the maturation and function of DCs.

Macrophages, an important member of the immune system, mainly possess immunological functions such as phagocytosis, secretion of cytokines and NO. It has been reported that activated macrophages kill pathogenic microorganisms and apoptotic cells directly, or release pro-inflammatory cytokines and NO, to mediate adaptive immune response [19]. In addition, macrophages also belong to APCs and can exert antigen-presenting function via up-regulation of MHC molecules and co-stimulatory molecules [20–22]. Hence, developing a safe and effective polysaccharide that can activate macrophages and enhance its immunomodulatory function is of high importance to the human health.

Toll-like receptors (TLRs) are the critical membrane receptor of immune cells, which are the binding receptor of most natural polysaccharides [23,24]. TLRs-induced signaling transduction pathways, such as MAPKs and NF- κ B signaling pathways ultimately result in the activation of APCs and initiation of the immune response of the host.

Furthermore, many polysaccharides possessed immunomodulatory activity *in vitro* and *in vivo*, by activating macrophages, DCs and T cells, regulating their phagocytic activity, phenotype and secretion of inflammatory cytokines [25–27]. In our previous study, we reported the structure of a new water-soluble polysaccharide (ASPW80-1) from the pulp tissues of custard apples and its biological activities. It is found that ASPAW80-1 possessed antioxidant activity and immunoregulatory effect by stimulating murine splenic lymphocyte proliferation [28]. However, the mechanism of the immunomodulatory activity of the polysaccharides from *Annona squamosa* L. remains unknown. The structure of ASPA80-1 and ASPW80-1 was different. ASPA80-1 had a higher proportion of galactose than ASPW80-1. It has been reported that polysaccharides rich in galactose exhibited better immunomodulatory activity on macrophages [29]. In addition, numerous studies reported that heteropolysaccharide possessed immune booster effects *in vitro* and *in vivo* [30,31]. In this study, we investigated the structural characterization and the immunomodulatory activity of the novel heteropolysaccharide (ASPA80-1). Furthermore, the possible mechanism was also explored, by which ASPA80-1 activated RAW264.7 cells and promoted DCs maturation.

2. Materials and methods

2.1. Materials and reagents

A. squamosa was purchased from Guangzhou Tianhe fruit wholesale market, Guangzhou, China. The pulp material was identified by Professor R.M. Yu, College of Pharmacy, Jinan University, China. Standard monosaccharides and T-series dextrans were obtained from Sigma Chemical Co. (St. Louis, MO, USA). DEAE-52 cellulose and Sephadex G-100 were obtained from Whatman Ltd (Kent County, England). Sephacryl S-300 HR was obtained from Amersham Biosciences (Pharmacia, Uppsala, Sweden). The rmGM-CSF (214-14) and rmIL-4 (315-03) were obtained from PeproTechInc (Rocky Hill, NJ, USA). Anti-CD11c-FITC, anti-MHC II-PE, anti-CD86-FITC and anti-CD11c-APC antibodies were purchased from eBioscience (San Diego, CA, USA). Neutral red was purchased from Amresco (Albany, NY, USA) and the NO assay kit was supplied by the Beyotime Institute of Biotechnology (Haimen, China). Lipopolysaccharide (LPS) and FITC-dextran were purchased from Sigma–Aldrich (St. Louis, MO, USA). Anti- β -actin and anti-GAPDH antibodies were obtained from Biosharp (Beijing, China). Anti-Histone-H3 antibody was obtained from Proteintech (Wuhan, China). MAPK family antibody sampler kit and NF- κ B pathway sampler kit were purchased from Cell Signaling Technology (Beverly, MA, USA). Other chemicals and reagents were of analytical grade.

2.2. Extraction, isolation and purification of ASPA80-1

The dried pulp tissues of *A. squamosa* (500 g) were defatted with 95% ethanol (1:7, w/v) for 3 h. After that, the tissues were filtered and dried at 50 °C. The dried powder was extracted with 10 L of a solution of simulated gastric juice (pH 1.5) at 37 °C for 4 h according to the method described by reference [32]. The simulated gastric juice contained sodium chloride (2.16 g/L), potassium dihydrogen phosphate (0.63 g/L), hydrochloric acid (1.34 g/L), potassium chloride (0.39 g/L), calcium chloride (0.12 g/L) and pepsin (0.53 g/L). The obtained extract was collected and centrifuged at 8000 rpm for 15 min. Thereafter, the supernatant was concentrated at 60 °C and precipitated with absolute ethanol (4 times volume) at 4 °C overnight. The precipitate was then re-dissolved in distilled water and concentrated to remove excess ethanol. The concentrated solution was deproteinized with Sevag reagent (chloroform/n-butanol = 4:1, v/v) 6 times for 15 min each [33]. The resulting solution was concentrated, then dialyzed against distilled water for 48 h. Finally, the solution was lyophilized as the crude polysaccharide (ASPA80).

ASPA80 (150 mg) was dissolved in 8 mL of deionized water, centrifuged and filtered through a 0.45 µm filter. The solution was injected into a column of DEAE-cellulose-52 (2.6 × 40.0 cm) and eluted stepwise with a NaCl linear gradient (0–0.8 M) at a flow rate of 0.8 mL/min. Each fraction was monitored at 490 nm by the phenol-sulfuric acid method, and the main polysaccharide fractions (ASPA80-S1) were pooled, dialyzed and lyophilized. ASPA80-S1 was further purified using a Sephadex G-100 column (1.6 × 80.0 cm) and Sephacryl S-300 HR (1.2 × 100.0 cm) eluted with deionized water at a flow rate of 0.5 mL/min. The resultant fraction was concentrated and freeze-dried to afford a purified polysaccharide (ASPA80-1).

2.3. Measurement of homogeneity and average molecular weight

The homogeneity and average molecular weight of ASPA80-1 were determined using high-performance gel-permeation chromatography (HPGPC) by an Agilent 1100 HPLC system equipped with a Shodex OHPak SB-804HQ column (8.0 × 300 mm) and a differential refractive index detector [34]. A sample solution (20 µL) was injected in each run, with 0.1 M NaCl as the mobile phase, at a flow rate of 1.0 mL/min. A standard curve of the logarithm of relative molecular weight (MW) related to retention time (t) was established using a dextran series (3, 7, 10, 70 and 200 kDa). The retention time of the ASPA80-1 was plotted on the same graph and the average molecular weights were calculated from the standard curve ($\log M_w = -1.0249t + 12.9394$, $R^2 = 0.9989$) [35].

2.4. Monosaccharide composition analysis

ASPA80-1 (5 mg) was hydrolyzed in 2 mL of 2 M TFA for 5 h at 110 °C. Thereafter, the excess TFA was removed by evaporation on a water bath at 40 °C and co-distilled with MeOH. The monosaccharide content was measured using high performance anion exchange chromatography (HPAEC-PAD). The hydrolysate (1 mg) was dissolved in distilled water (1 mL) and then filtered using a 0.45 µm filter. The solution (20 µL) was injected into HPAEC-PAD on the Dionex ICS-2500 system and eluted with a mixture of water and 200 mM NaOH in a volume ratio of 92 : 8 [36].

2.5. Partial acid hydrolysis

ASPA80-1 (30 mg) was dissolved in 30 mL of 0.05 M TFA and kept at 100 °C for 6 h, and then the hydrolysate was dialyzed with distilled water for 48 h. The fraction outside the dialysis sack was collected and the excess TFA was removed by co-distillation with MeOH. Thereafter, the fraction was concentrated to dryness (Fraction 1). The fraction in the dialysis sack was dried by evaporation and then hydrolyzed with 30 mL of 0.5 M TFA. The hydrolysate was dialyzed and the fraction outside the dialysis sack (Fraction 2) and the fraction in the sack (Fraction 3) were collected, respectively. Afterwards, fractions 1–3 were hydrolyzed with 2 M TFA (5 mL) at 100 °C for 5 h and evaluated by HPAEC-PAD.

2.6. Periodate oxidation and smith degradation

ASPA80-1 (15 mg) was swelled in 5 mL of distilled water, and then 25 mL of 15 mM NaO₄ was added. The solution (30 mL) was drawn at 6 h intervals in the dark at 4 °C, then diluted to 5 mL with water and measured in a spectrophotometer at 223 nm until the absorbance became stable [37]. The consumption of HIO₄ was measured using a spectrophotometric method and the production of formic acid was determined by titration with 0.051 M NaOH. The reaction residue was dialyzed against tap water for 48 h and distilled water for 24 h. The non-dialysate was concentrated, reduced with NaBH₄ (100 mg) for 24 h at room temperature, and then neutralized to pH 6.0 with 0.1 M HOAc. After dialysis and concentration, the retentate was hydrolyzed with 2.0 M TFA (5 mL) for 12 h at 100 °C. Finally, the product was analyzed with HPAEC-PAD.

2.7. Methylation and GC-MS analysis

ASPA80-1 was methylated according to the reported method with minor modifications [38]. ASPW80-1 (7 mg) was added to a flask containing 5 mL of DMSO and stirred for 1 h. Then, 200 mg of NaOH and 5 mL of DMSO were added to the flask, and mixed for 1.5 h. CH₃I (1.6 mL) was then added in two batches to the mixture and stirred for 2 h. Finally, the reaction was terminated by adding 1 mL of distilled water and the mixture was extracted with chloroform three times. Repeat methylation until the complete methylation sample was achieved, which can be confirmed by the disappearance of the OH band in the region of 3500–3100 cm⁻¹ in IR spectrometry. After

hydrolysis, reduction, and acetylation, the product was analyzed by GC-MS (Agilent Technologies Co., Ltd., USA). The analysis conditions were as follows: the temperature was increased from 100 to 180 °C at a rate of 5 °C/min, then increased to 280 °C at 10 °C/min and maintained for 20 min.

2.8. FT-IR spectroscopic analysis

ASPA80-1 samples (2–3 mg) were ground to a fine powder and analyzed using the potassium bromite pellet method with a Fourier transform infrared (FT-IR) spectrophotometer in the 500–4000 cm^{-1} vibration region.

2.9. NMR spectroscopic analysis

ASPA80-1 (40 mg) was dissolved in 0.5 mL of D_2O . After that, NMR (^1H NMR and ^{13}C NMR) were recorded by Bruker AMX-500 NMR spectrometer. The parameters of ^1H NMR experiment are presented as follows: pulse program zg30, a spectral width of 8.22 kHz, an acquisition time of 4 s, a relaxation delay of 1 s, for 64 scans. For 100 MHz proton decoupled ^{13}C NMR experiment, the parameters are presented as follows: pulse program zgpg30, a spectral width of 24.0 kHz, an acquisition time of 1.36 s, a relaxation delay of 1 s, for 73,728 scans.

2.10. Cell lines and cell culture

RAW264.7 cells were purchased from the American Type Culture Collection (ATCC). The cells were cultured in a DMEM medium supplemented with 10% FBS plus 1% Penicillin/Streptomycin and incubated in a humidified incubator with 5% CO_2 at 37 °C.

DCs were generated using a modified reference protocol from references [39,40]. Briefly, bone marrow hematopoietic cells (BMHCs) were flushed from the femurs and tibias of sacrificed mice. Then BMHCs were cultured in RPMI 1640 complete medium containing 10 ng/mL rmGM-CSF and 10 ng/mL rIL-4. Two-thirds of the medium was changed to a fresh complete medium containing 10 ng/mL GM-CSF and 10 ng/mL IL-4 on day 3 and day 5, respectively. On day 6, nonadherent and loosely adherent DCs were harvested by vigorous pipetting.

2.11. Phenotype analysis

RAW264.7 cells (3×10^4 cells/well) were seeded in 96-well plates and DCs (5×10^4 cells/well) were seeded in 12-well plates. Then, cells were treated with serial concentrations of ASPA80-1 for 24 h. RAW264.7 cells were incubated with FITC-CD86 or PE-MHC II antibodies for 30 min at 4 °C, while DCs were incubated with APC-CD11c plus FITC-CD86 or FITC-CD11c plus PE-MHC II antibodies for 30 min at 4 °C. Finally, cells were collected and analyzed by BD FACSCanto flow cytometer.

2.12. Nitrite production assay

RAW264.7 cells (1×10^6 cells/mL) were seeded in 96-well plates and stimulated with serial concentrations of ASPA80-1 or LPS (1 $\mu\text{g}/\text{mL}$) for 24 h. Furthermore, the supernatant (50 μL) was collected and mixed with Griess reagent A (50 μL) and Griess reagent B (50 μL) at room temperature (RT) for 10 min. NO production was measured at 540 nm with a Synergy™ HT Multi-function Microplate Reader.

2.13. Phagocytic assay

2.13.1. Neutral red granules phagocytosis assay

RAW264.7 cells (1.5×10^4 cells/well) were seeded in 96-well plates and treated with different concentrations of ASPA80-1 or LPS (1 $\mu\text{g}/\text{mL}$) for 24 h. Then, 100 μL of 0.1% neutral red solution was added to each well and incubated for 30 min. Finally, 150 μL of cell lysate (acetic acid/ethanol = 1:1, v/v) was added to each well to extract the dye phagocytized by RAW264.7 cells. The absorbance was read at 540 nm with a Synergy™ HT Multi-function Microplate Reader.

2.13.2. FITC-dextran phagocytosis assay

RAW264.7 cells (1.5×10^4 cells/dish) were seeded in confocal dish and DCs (5×10^4 cells/mL) were seeded in 12-well plates, and then they were treated with ASPA80-1 or LPS (1 $\mu\text{g}/\text{mL}$) for 24 h. After 24 h, 1 mg/mL FITC-dextran was added to co-culture for 1 h. On the one hand, RAW264.7 cells were fixed with 4% paraformaldehyde for 20 min and incubated with diamidino-phenyl-indole (DAPI) for 5 min. Then the fluorescence was visualized by ZEISS LSM880 with an AiryScan laser confocal microscope. On the other hand, DCs were stained with APC conjugated anti-CD11c antibody at 4 °C for 30 min. Double-stained DCs were analyzed by BD FACSCanto flow cytometer.

2.14. Western blot

RAW264.7 cells (2×10^5 cells/well) or DCs (2×10^5 cells/well) were seeded in 6-well plates and treated with different concentrations of ASPA80-1. And then, the cells were harvested and proteins were extracted with SDS lysis buffer to serve as the total cell

extract. The nuclear protein was extracted using a nuclear and cytoplasmic protein extraction kit according to the manufacturer's protocol. Furthermore, the protein concentration was determined using a BCA kit. Proteins were loaded into each lane and separated using SDS polyacrylamide gel electrophoresis (SDS-PAGE). Then the separated proteins were transferred onto the PVDF membranes and the membranes were blocked with 5% skimmed milk for 2 h. The membranes were incubated overnight with appropriate primary antibodies and incubated with goat anti-mouse or rabbit HRP secondary antibody at RT for 2 h. The band intensity was analyzed after it was developed using ECL detection reagents (Millipore Co., Billerica, Massachusetts, USA).

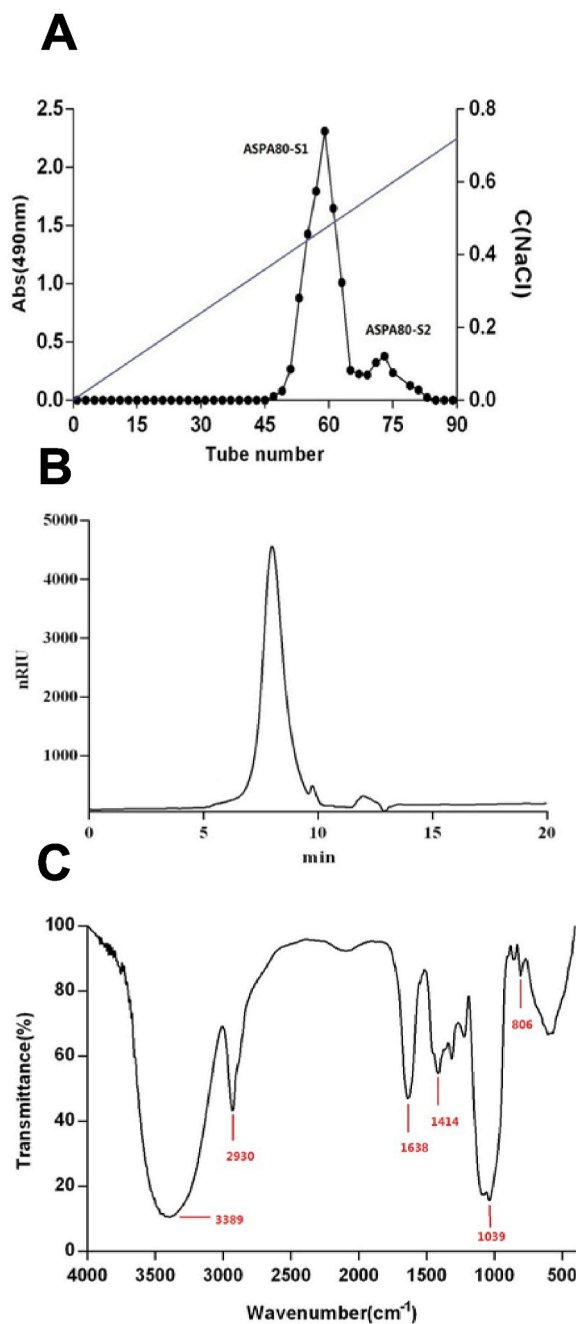


Fig. 1. The profiles and spectrum of ASPA80-1. (A) Elution profile of crude polysaccharide ASPA80 on DEAE-cellulose 52 column chromatography. (B) HPGPC profile of ASPA80-1. (C) FT-IR spectrum of ASPA80-1.

2.15. Statistical analysis

The results are expressed as means \pm standard deviation (SD) and all experiments were done in triplicate. Statistical analysis was determined by one-way ANOVA followed by Dunnett's post-test using GraphPad Prism 9.1.0. $p < 0.05$ was regarded as a level of statistically significant differences.

3. Results

3.1. Isolation, purification and general properties of ASPA80-1

The crude polysaccharide (4.35 g) was obtained at a 0.87% yield from the raw plant material. ASPA80 was separated and fractionated on a DEAE-cellulose 52 column stepwise with distilled water and a NaCl gradient (0–0.8 M) to obtain two elution peaks (ASPA80-S1 and ASPA80-S2) (Fig. 1A). ASPA80-S1 was further purified using a Sephadex G-100 column and Sephacryl S-300 HR eluted with distilled water. The eluate was combined, concentrated, dialyzed and lyophilized to obtain the purified polysaccharide (ASPA80-1). The yield of ASPA80-1 from crude polysaccharides was 32.2%. The total carbohydrate content of ASPA80-1 was 95.36% (w/w) and the m-hydroxybiphenyl colorimetric test result was negative. The uronic acid content of ASPA80-1 was below the limit of detection. ASPA80-1 was a white powder which is soluble in water and DMSO. The optical rotation of ASPA80-1 was $[\alpha]_D^{20} = -26^\circ$ (c 1.0, 28 °C, H₂O).

3.2. Homogeneity and average molecular weight of ASPA80-1

ASPA80-1 exhibited a single and symmetrical narrow peak with an elution time of 8.001 min, as revealed by HPGPC analysis (Fig. 1B), thereby confirming its homogeneity. Based on the calibration equation derived from linear regression of the calibration curve, the average molecular weight of ASPA80-1 was approximately 5.48×10^4 Da according to the retention time.

3.3. Structural elucidation of ASPA80-1

The monosaccharide composition of ASPA80-1 was presented in Table 1. The analysis indicated that ASPA80-1 was a heteropolysaccharide and consisted of L-rhamnose, L-arabinose, D-galactose and D-glucose in the molar ratio of 1.00 : 8.23 : 2.31 : 1.49 as revealed by HPAEC-PAD analysis. The composition analyses of fraction 3 in Table 1 indicated that the backbone of ASPA80-1 was composed of L-rhamnose and D-galactose in the molar ratio of 3.14 : 1.00. The branched structure of ASPA80-1 was made up of L-arabinose, L-rhamnose, D-galactose and terminated with L-rhamnose as indicated by the analysis results of fractions 2 and fractions 3 (Fig. 2). The periodate-oxidized products were fully hydrolyzed and analyzed by HPAEC-PAD after periodate oxidation. The results shown in Table 1 demonstrated that there were no L-rhamnose, D-glucose, D-galactose in the oxidation products. It could be inferred that linkages of L-rhamnose, D-glucose and D-galactose were (1 \rightarrow), (1 \rightarrow 2), (1 \rightarrow 6), (1 \rightarrow 2,6), (1 \rightarrow 4) and (1 \rightarrow 4,6), which might be oxidized to produce glycerol and erythritol [41,42]. The presence of L-arabinose revealed that some residues of L-arabinose were (1 \rightarrow 3)-linked, (1 \rightarrow 2,3)-linked, (1 \rightarrow 2,5)-linked or (1 \rightarrow 3,5)-linked, which could not be oxidized. ASPA80-1 showed abundant HIO₄ uptake during oxidation. The presence of formic acid in the product indicated the existence of a (1 \rightarrow)-linked or (1 \rightarrow 6)-linked monosaccharide. The consumption of HIO₄ (0.1238 mmol) was twice that of the production of formic acid (0.0145 mmol), indicating the existence of large amounts of monosaccharide that was (1 \rightarrow 4)-linked, (1 \rightarrow 4,6)-linked, (1 \rightarrow 2)-linked or (1 \rightarrow 2,6)-linked.

3.4. Methylation and GC-MS analysis of ASPA80-1

Methylation analysis by GC-MS provided more structural information for ASPA80-1. Six homogeneous peaks of the fully methylated alditol acetates were obtained from the GC-MS analysis. The results indicated the presence of six components, namely, 2,3,5-Me₃-Ara, 2,5-Me₂-Ara, 2-Me-Ara, 2,3,4-Me₃-Gal, 2,3,6-Me₃-Glc and 3,4-Me₂-Rha, in a molar ratio of 1.95 : 4.19 : 2.05 : 2.24 : 1.30 : 1.00 (Table 2). According to their retention times, by comparison with mass spectrum patterns from the literature, and on the basis of the standard data in the CCRC Spectral Database for PMAAs, the linkages of L-rhamnose were determined to be (1 \rightarrow 2), the linkage of D-galactose was determined to be (1 \rightarrow 6), the linkage of D-glucose was determined to be (1 \rightarrow 4) and the linkages of L-arabinose were

Table 1
HPAEC-PAD analysis for ASPA80-1 degradation products.

	Molar ratios			
	L-rhamnose	L-arabinose	D-galactose	D-glucose
ASPA80-1	1.00	8.23	2.31	1.49
Fraction 1	1.00	n.d.	n.d.	n.d.
Fraction 2	1.00	n.d.	n.d.	1.29
Fraction 3	3.14	0.01	1.00	n.d.
Smith degradation	n.d.	1.00	n.d.	n.d.

^and, not detected.

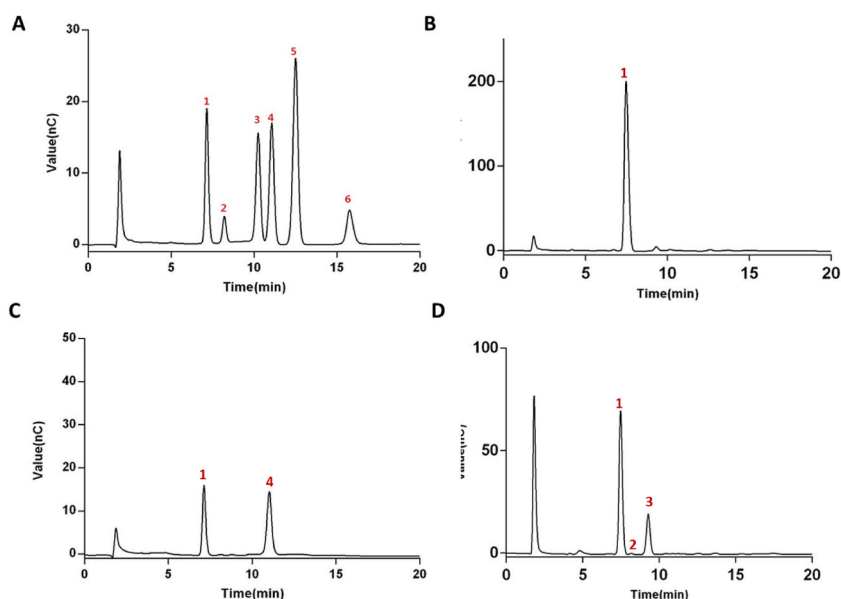


Fig. 2. HEPAC-PAD for monosaccharide compositional analysis of ASPA80-1. (A) Standard monosaccharides; (B) Effect of 0.05 mol/L TFA on ASPA80-1; (C) Effect of 0.5 mol/L TFA on ASPA80-1; (D) Effect of 2 mol/L TFA on ASPA80-1. Peaks in: 1, rhamnose; 2, arabinose; 3, galactose; 4, glucose; 5, xylose; 6, fructose.

Table 2

Methylation analysis of ASPA80-1.

Methylation Sugar	Molar ratio	Mass fragments (m/z)	Linkage type
2,3,5-Me ₃ -Ara	1.95	58, 71, 87, 101, 117, 129, 145, 161	T→
2,5-Me ₂ -Ara	4.19	58, 87, 99, 117, 129, 159, 233	1 → 3
2-Me-Ara	2.05	59, 72, 99, 117, 127, 156, 174, 186, 261	1 → 3,5
2,3,4-Me ₃ -Gal	2.24	58, 71, 87, 101, 117, 129, 189	1 → 6
2,3,6-Me ₃ -Glc	1.30	87, 99, 101, 117, 129, 161	1 → 4
3,4-Me ₂ -Rha	1.00	87, 129, 131, 189, 237, 281	1 → 2

determined to be (1→), (1 → 3) and (1 → 3,5). There was a good correlation between the terminal and branched residues, and the molar ratio of these residues was in accordance with the monosaccharide composition of ASPA80-1 as described above.

3.5. UV and FT-IR spectroscopic analysis of ASPA80-1

UV scanning at 280 and 260 nm detected no absorbance peaks, indicating that ASPA80-1 contained no protein or nucleic acid [43]. The infrared spectrum of ASPA80-1 revealed the major functional groups and the chemical bonds (Fig. 1C). In the FT-IR spectrum, the characteristic bands in the regions of 3389, 2930 and 1638 cm^{-1} belonged to O-H bending, C-H bending and C=O bending, respectively. The peaks at ground 1400–1200 cm^{-1} also indicated the characteristic absorption of C-H bands. The band at 1414 cm^{-1} was due to C–O bending and the bands at 1039–1071 cm^{-1} indicated pyranose. The characteristic absorptions at 806 and 861 cm^{-1} indicated that α - and β -configurations were present simultaneously. There was no absorption at 1740 cm^{-1} , indicating no uronic acid in the polysaccharide structure [44,45].

3.6. NMR spectroscopic analysis of ASPA80-1

To get high-resolution characterization of structure, ASPA80-1 was analyzed via NMR, as shown in Fig. 3A and B. The signals of the ^1H and ^{13}C NMR spectra showed the typical characters of polysaccharides. The ^1H NMR spectrum of ASPA80-1 was typically recognized between 3.5 and 5.5 ppm which confirmed the structural feature of monosaccharide residues. The low-field position of the anomeric protons signal at > 5.0 ppm suggested the existence of α -configuration. Conversely, the anomeric protons signal at < 5.0 ppm was assigned as β -configuration according to the existing literatures [46]. ASPA80-1 had six main anomeric proton signals at 5.43, 5.36, 5.34, 5.30, 5.27 and 4.61 ppm. The result indicated that ASPA80-1 mainly contained α -configurations with minor β -configurations. The ^{13}C NMR spectrum revealed carbon resonances with chemical shifts characteristic for ASPA80-1. There were also six obvious chemical shifts of anomeric carbon found at 109.11, 107.72, 107.15, 106.64, 98.56 and 98.08 ppm.

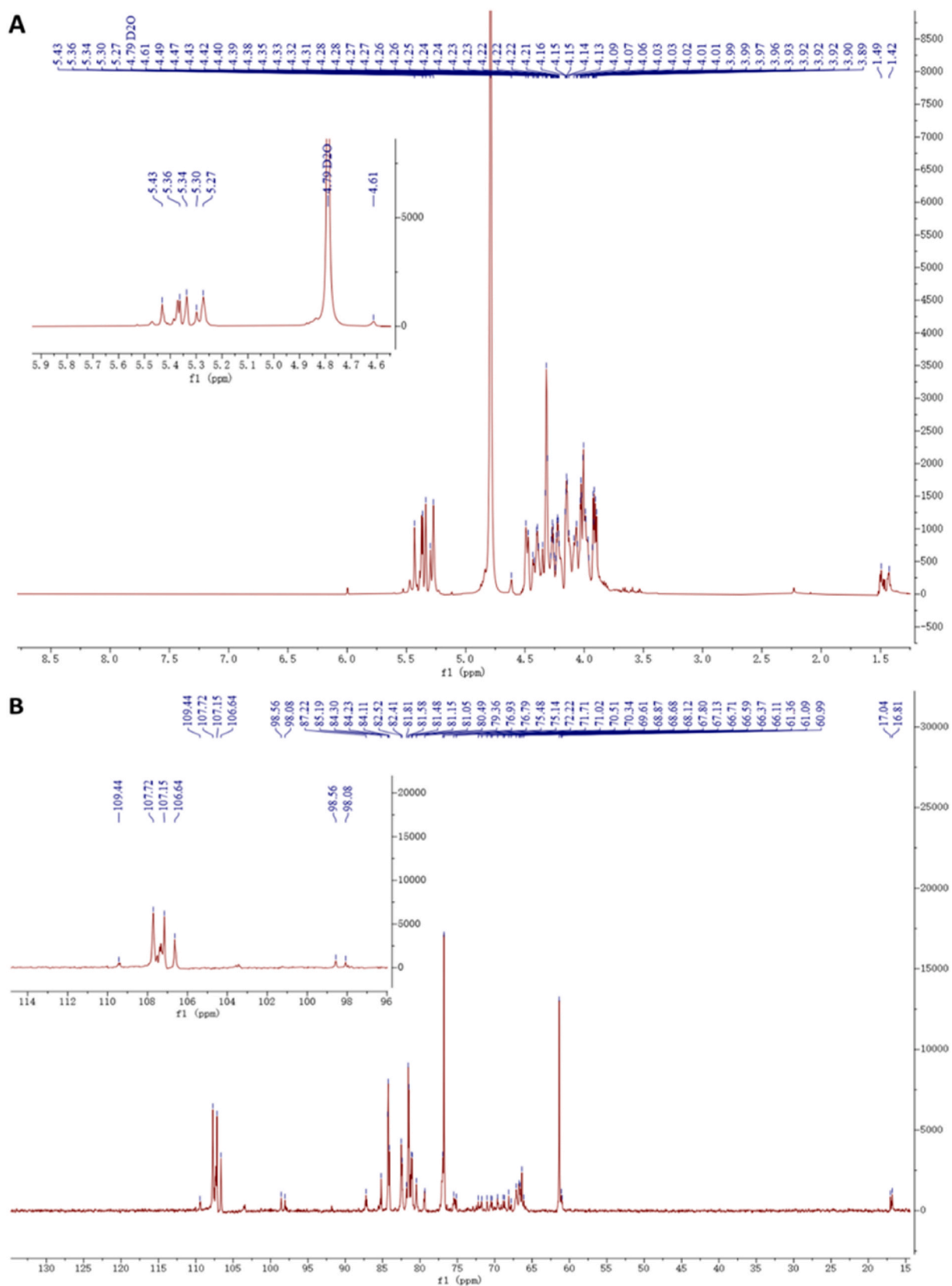


Fig. 3. NMR spectra of ASPA80-1. (A) ^1H -NMR spectrum; (B) ^{13}C NMR spectrum of ASPA80-1.

3.7. Effect of ASPA80-1 on the activation of RAW264.7 cells

In this study, RAW264.7 cells were used as a cell model to investigate the function of macrophages. Neutral red granules and FITC-dextran were applied to measure the phagocytic ability of RAW264.7 cells. As depicted in Fig. 4A, the uptake of neutral red on RAW264.7 cells treated with ASPA80-1 from 11.11 to 900 µg/mL was higher than that of the control group, especially at the concentration from 100 to 900 µg/mL ($p < 0.01$). Similarly, FITC-dextran uptake was found under the confocal microscope in the ASPA80-1-treated and LPS-treated RAW264.7 cells. As indicated in Fig. 4B, ASPA80-1 caused a significant increase in the green fluorescence intensity of macrophages when compared to that of cells in the untreated group, which was consistent with the results of the neutral red phagocytosis assay.

Then, the NO production level was measured to evaluate the effect of ASPA80-1 on the activation of macrophages. As shown in Fig. 4C, NO production was low in untreated RAW264.7 cells, while it increased significantly after the intervention of ASPA80-1. ASPA80-1 increased the secretion of NO dose-dependently, especially at concentrations between 100 and 900 µg/mL, approximately 22, 37 and 54 times as much as the negative control group ($p < 0.01$).

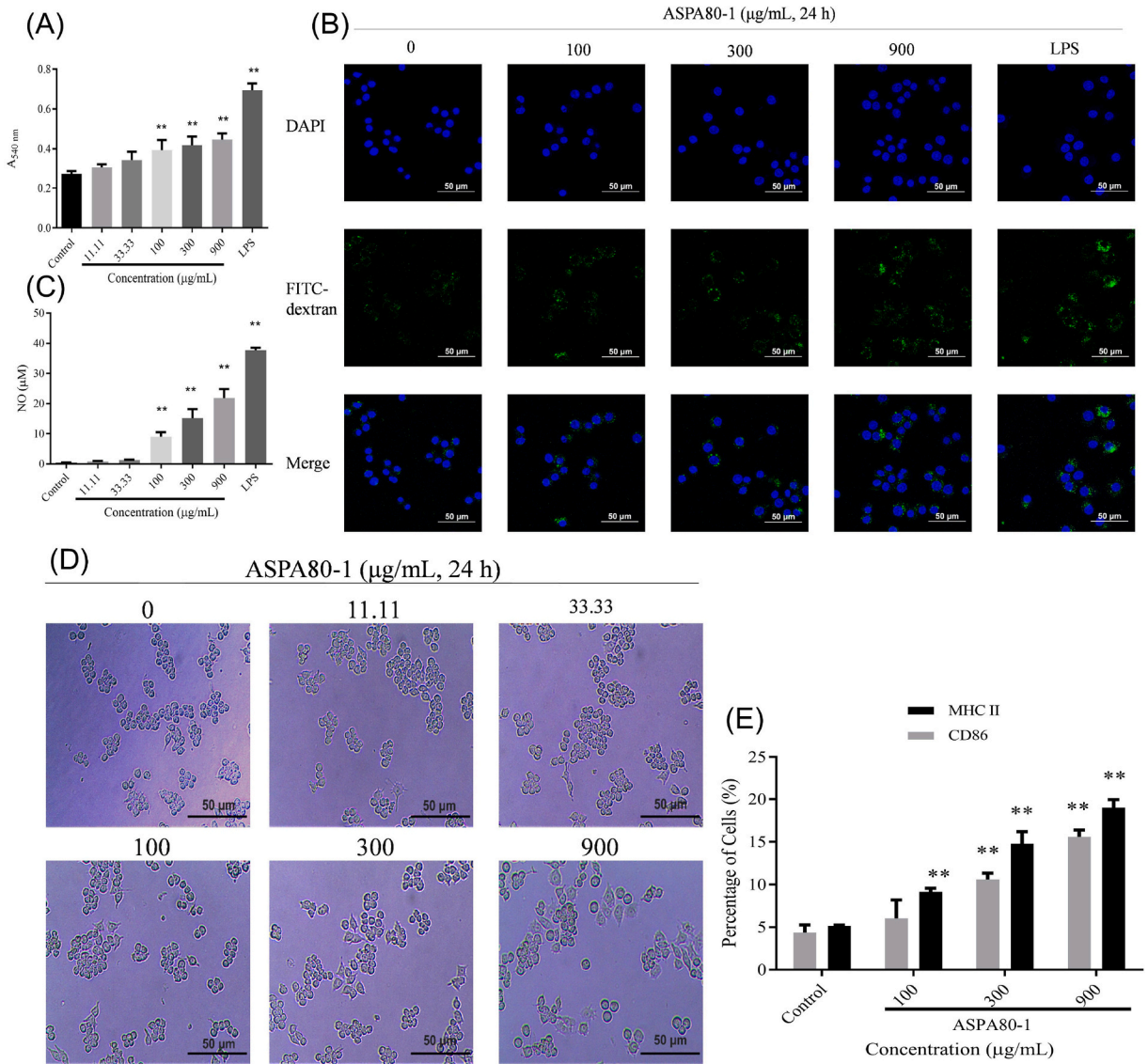


Fig. 4. ASPA80-1 promoted the activation of RAW264.7 cells. RAW264.7 cells were intervened with different concentrations of ASPA80-1 or LPS (1 µg/mL) for 24 h. The phagocytosis of RAW264.7 cells was improved by ASPA80-1 in (A) neutral red phagocytosis assay and (B) FITC-dextran phagocytosis assay (scale bar = 50 µm). (C) The level of NO in RAW264.7 cells was detected by the Griess reagent. (D) Morphology changes of RAW264.7 cells (scale bar = 50 µm). (E) The expression level of MHC II and CD86 was measured by a flow cytometer. The results were expressed as means ± SD (n = 3). ** $p < 0.01$ versus the negative control.

According to Fig. 4D, the typical morphology of RAW264.7 cells was round, and just a few cells were fusiform in the control group. However, after treatment with ASPA80-1 for 24 h, RAW264.7 cells showed polygonal and dendritic-like morphology. Furthermore, as depicted in Fig. 4E, RAW264.7 cells stimulated with ASPA80-1 (100, 300 and 900 $\mu\text{g}/\text{mL}$) for 24 h displayed higher expression of MHC II and CD86 molecules when compared with the untreated group ($p < 0.01$).

3.8. Effect of ASPA80-1 on the maturation of DCs

As displayed in Fig. 5A, after being treated with ASPA80-1 for 24 h, DCs showed more dendrites and elongated protrusion, while non-treated DCs exhibited slightly rough surface and small dendrites. Furthermore, with the flow cytometer analysis, the percentages of CD86 and MHC II positive DCs in the ASPA80-1-treated group were higher than in the control group (Fig. 5B). At the same time, the median fluorescence intensity (MFI) of DCs was lower than the control group ($p < 0.01$), which had the same trend as the positive drug LPS (Fig. 5C).

3.9. Effect of ASPA80-1 on MAPKs and NF- κB signaling pathways in RAW264.7 cells and DCs

As shown in Fig. 6A and B, ASPA80-1 increased the expression of p-ERK, p-JNK, p-P38 and p-NF- κB in RAW264.7 cells. Moreover, ASPA80-1 up-regulated the expression of the NF- κB in the nucleus of RAW264.7 cells (Fig. 6C). It was suggested that ASPA80-1 activated the MAPKs and NF- κB signaling pathways and promoted the translocation of NF- κB from the cytoplasm to the nuclei.

Similarly, the increased expression of p-JNK, p-P38 and p-NF- κB was found in the ASPA80-1 treated DCs but not p-ERK (Fig. 7A and B). Regarding the translocation of NF- κB in ASPA80-1-treated DCs, we also found that ASPA80-1 increased the expression of NF- κB

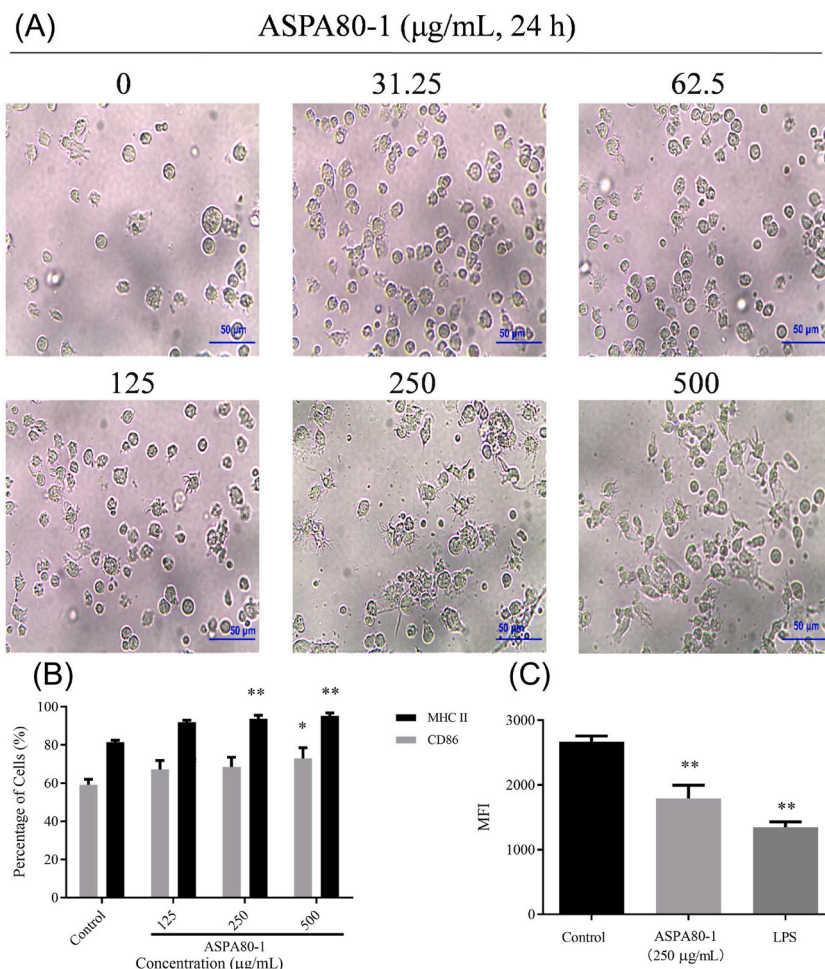


Fig. 5. ASPA80-1 induced the maturation of DCs. DCs were treated with various concentrations of ASPA80-1 or LPS (1 $\mu\text{g}/\text{mL}$) for 24 h. (A) Morphology changes of DCs (scale bar = 50 μm). (B) The expression level of CD86 and MHC II on DCs was measured by a flow cytometer. (C) The phagocytosis of FITC-dextran was detected by a flow cytometer. Data are presented as mean \pm SD ($n = 3$). * $p < 0.05$, ** $p < 0.01$ versus the negative control.

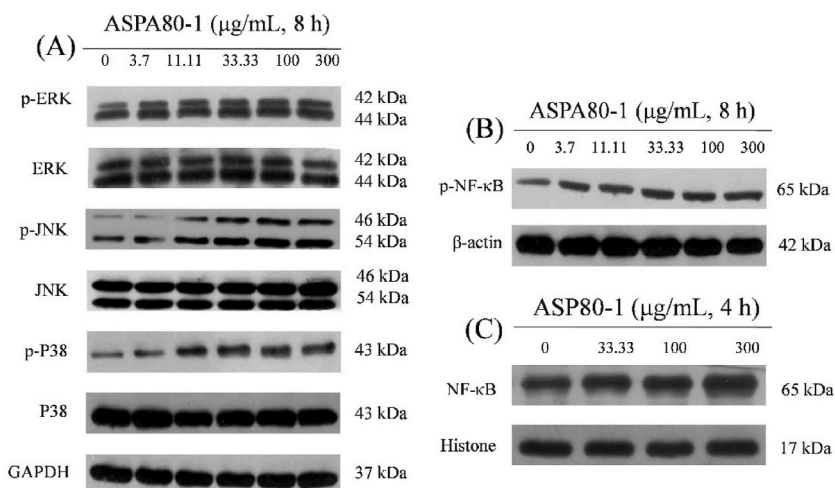


Fig. 6. ASPA80-1 activated the MAPKs and NF-κB signaling pathway in RAW264.7 cells. (A, B) Effect of ASPA80-1 on the MAPKs and NF-κB signaling pathways in RAW264.7 cells. (C) Effect of ASPA80-1 on the NF-κB in RAW264.7 cell nucleus. Refer to [Supplementary Figs. S1–3](#) for uncropped version of the graph.

in the nucleus of DCs ([Fig. 7C](#)). The results suggested that ASPA80-1 could activate MAPKs and NF-κB signaling pathways.

4. Discussion

Generally, the immunoenhancing activity of natural polysaccharides is correlated to its molecular weight, steric conformation, glycosidic bond, types of linkage, and side-chain distribution, among which the influences of molecular weight and monosaccharide composition are the most noticeable [52,53]. It has been previously shown that Glc, Gal, or Ara in the monosaccharide composition of polysaccharides was more likely to be recognized by cell membrane receptors, which trigger immune response [54]. Moreover, the appropriate molecular weight of polysaccharides between 5 and 100 kDa appeared to be more effective than those of high molecular weight in modulating the activity of immune cells [55]. The current study demonstrated that the average molecular weight of ASPA80-1 was 5.48×10^4 Da and the monosaccharide was mainly composed of Ara and Gal, and a slight amount of Glc and Rha, which may explain its much greater immunomodulatory activity. Meanwhile, a novel polysaccharide (MOP-3) isolated from the leaves of *Moringa oleifera* was composed of Ara, Glc and Gal with a molar ratio of 47.73 : 1.00: 57.65 and possessed good immunoenhancing activity [56]. Another polysaccharide (SSPA50-1) isolated from *Scapharca subcrenata* had an average molecular weight of 44.7 kDa and consisted of GalA, Glc, Gal, Man, Rib, Rha, Fuc, Xyl and Ara, which exhibited important immunomodulatory activity *in vitro* [57]. It has been well documented that heteropolysaccharide possessed immune booster effects *in vitro* and *in vivo*. Thus, the excellent immunomodulatory activity of ASPA80-1 may be related to the heteropolysaccharide with high branched structures.

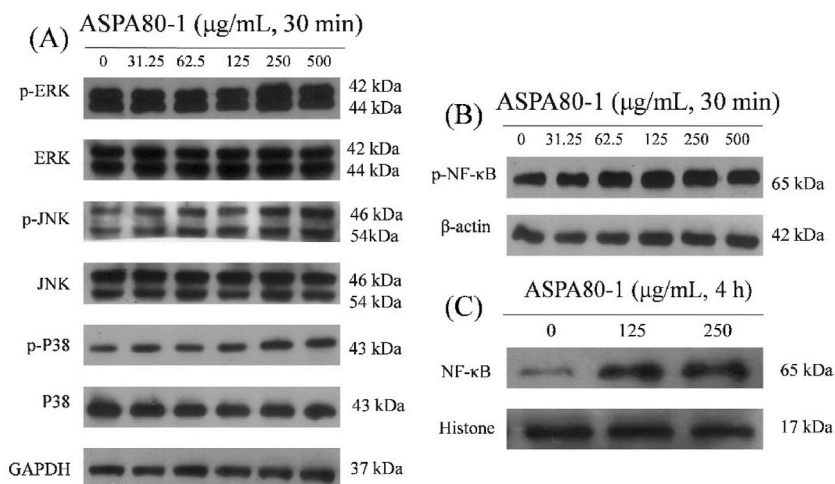


Fig. 7. ASPA80-1 activated the MAPKs and NF-κB signaling pathways in DCs. (A, B) Effect of ASPA80-1 on the MAPKs and NF-κB signaling pathways in DCs. (C) Effect of ASPA80-1 on the NF-κB in DCs nucleus. Refer to [Supplementary Figs. S4–6](#) for uncropped version of the graph.

NO is a bioactive chemokine produced by inducible nitric oxide synthase (iNOS) of macrophages, and it can damage microorganisms even tumor cells [48,49]. Phagocytic activity and NO secretion are essential feature of macrophages and polysaccharides can enhance their phagocytosis [47]. Neutral red granules, FITC-dextran and NO assays indicated that the phagocytosis of macrophages was enhanced after the stimulation with ASPA80-1 for 24 h. As one of the members of APCs, macrophages also possess antigen-presenting function. Dendrite-like morphology change and higher expression of MHC II and CD86 in the ASPA80-1-induced RAW264.7 cells indicated that ASPA80-1 could enhance the antigen-presenting function of macrophages. Mature DCs were characterized by dendritic-like morphology, higher expression of CD86 and MHC II membrane marker on DCs and weak phagocytosis. Our results showed that ASPA80-1 promoted the maturation of DCs and enhanced the antigen-presenting function of DCs.

To further investigate the possible mechanism involved in the activation of RAW264.7 cells and the maturation of DCs by ASPA80-1, we focused on the MAPKs and NF- κ B signaling pathways since it is reported that they are responsible for polysaccharides-induced activation of APCs [40,41]. As is shown in the results, MAPKs and NF- κ B signaling pathways were activated in ASPA80-1-treated RAW264.7 cells and DCs. The ERK activation is generally associated with cell survival and proliferation [42]. Referring to the unchanged expression level of p-ERK in ASPA80-1-treated DCs, it was possible that ASPA80-1 mainly focused on the maturation of DCs but not DCs survival and proliferation. Polysaccharides cannot enter cells directly due to their complicated structure and considerable molecular weight. It has been reported that toll-like receptors (TLRs) can bind with polysaccharides and activate the downstream signaling pathways, such as MAPKs and NF- κ B signaling pathways [50,51]. Therefore, the ASPA80-1-induced activation of RAW264.7 cells and maturation of DCs might be related to TLRs-mediated MAPKs and NF- κ B signaling pathways. The present study proposed the potential immunoregulatory mechanism of ASPA80-1 on macrophage activation and DCs maturation in Fig. 8.

In this study, we have constructed a stable extracted method to prepare ASPA80-1 and elucidated its structure. Then, it is clarified that ASPA80-1 promoted the activation of RAW264.7 cells and maturation of DCs *in vitro*. However, the activation of APCs mediated by MAPKs and NF- κ B signaling pathways and the specific target need further verification in the further. Furthermore, it is important to explore the immune-enhancing activity of ASPA80-1 *in vivo*, which will provide a research evidence to develop it as a potential immune-enhancing agent in functional foods.

5. Conclusions

In the present study, a novel heteropolysaccharide (ASPA80-1) was isolated from the pulp tissues of *A. squamosa*, mainly consisting of L-rhamnose, L-arabinose, D-galactose and D-glucose with an average molecular weight of 5.48×10^4 Da. The pharmacological assay showed that ASPA80-1 could activate APCs, including the activation of RAW264.7 cells and the maturation of DCs. The proposed mechanism of the ASPA80-1-induced activation of APCs might be related to TLRs-mediated MAPKs and NF- κ B signaling pathways. Based on these findings, ASPA80-1 may have potential applications in a novel nutraceutical to enhance host immune response by activating antigen-presenting cells.

Author contribution statement

Chunhua Huang: Conceived and designed the experiments; Performed the experiments; Analyzed and interpreted the data; Wrote the paper.

Wensong Tu: Conceived and designed the experiments; Performed the experiments; Analyzed and interpreted the data; Wrote the paper.

Man Zhang: Conceived and designed the experiments; Performed the experiments; Analyzed and interpreted the data; Wrote the paper.

Dan Peng: Performed the experiments; Analyzed and interpreted the data.

Jianhua Zhu: Performed the experiments; Analyzed and interpreted the data.

Zhongyi Guo: Performed the experiments.

Weijuan Huang: Performed the experiments.

Rongmin Yu: Conceived and designed the experiments; Contributed reagents, materials, analysis tools or data; Wrote the paper.

Liyang Song: Conceived and designed the experiments; Contributed reagents, materials, analysis tools or data; Wrote the paper.

Yurong Wang: Conceived and designed the experiments; Contributed reagents, materials, analysis tools or data; Wrote the paper.

Data availability statement

Data included in article/supplementary material/referenced in article.

Funding

This study was supported by the National Natural Science Foundation of China of China (No. 82174019), and Guangzhou Science and Technology Plan Project (No. 202102020312).

Declaration of competing interest

The authors declare the following financial interests/personal relationships which may be considered as potential competing

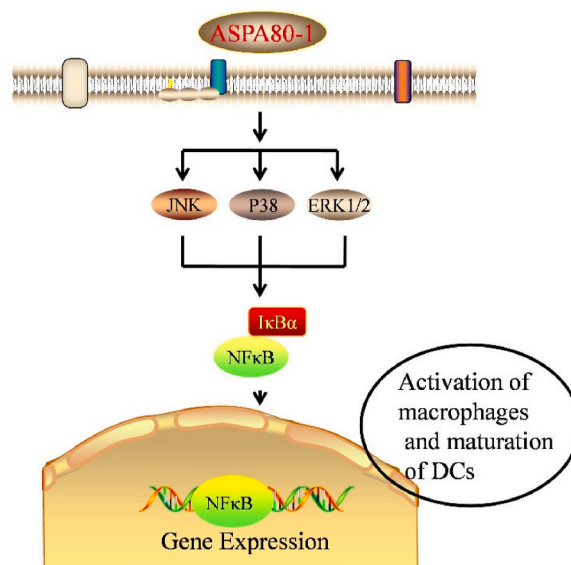


Fig. 8. Illustration of the proposed mechanism of ASPA80-1-induced macrophage activation and DCs maturation.

interests:

Prof. Rongmin Yu is a Pharma/Tox Advisory Board Member of Heliyon. Other authors declare that they have no known competing financial interests or personal relationships that could have appeared to influence the work reported in this paper.

Appendix A. Supplementary data

Supplementary data to this article can be found online at <https://doi.org/10.1016/j.heliyon.2023.e18521>.

References

- [1] R. Chen, J. Xu, W. Wu, Y. Wen, S. Lu, H.R. El-Seedi, C. Zhao, Structure-immunomodulatory activity relationships of dietary polysaccharides, *Curr. Res. Food Sci.* 5 (2022) 1330–1341.
- [2] B. Yang, Y. Luo, Y. Sang, J. Kan, Isolation, purification, structural characterization, and hypoglycemic activity assessment of polysaccharides from *Hovenia dulcis* (Guai Zao), *Int. J. Biol. Macromol.* 208 (2022) 1106–1115.
- [3] W. Zhang, B. Hu, M. Han, Y. Guo, Y. Cheng, H. Qian, Purification, structural characterization and neuroprotective effect of a neutral polysaccharide from *Sparassis crispa*, *Int. J. Biol. Macromol.* (2022), 201447 pages 389–399.
- [4] J. Garcia, F. Rodrigues, M.J. Saavedra, F.M. Nunes, G. Marques, Bioactive polysaccharides from medicinal mushrooms: A review on their isolation, structural characteristics and antitumor activity, *Food Biosci.* (2022), 101955.
- [5] L. Wang, K. Zhang, S. Han, L. Zhang, H. Bai, F. Bao, Y. Zeng, J. Wang, H. Du, Y. Liu, Z. Yang, Constituents isolated from the leaves of *Glycyrrhiza uralensis* and their anti-inflammatory activities on LPS-induced RAW264.7 cells, *Molecules* 24 (10) (2019) 1923.
- [6] I.A. Schepetkin, M.T. Quinn, Botanical polysaccharides: macrophage immunomodulation and therapeutic potential, *Int. Immunopharmacol.* 6 (3) (2006) 317–333.
- [7] A. Tariq, S. Mussarat, M. Adnan, Review on ethnomedicinal, phytochemical and pharmacological evidence of Himalayan anticancer plants, *J. Ethnopharmacol.* 164 (2015) 96–119.
- [8] M.G. Shehata, M.M. Abu-Serie, N.M. Abd El-Aziz, S.A. El-Sohaimy, Nutritional, phytochemical, and in vitro anticancer potential of sugar apple (*Annona squamosa*) fruits, *Sci. Rep.-UK* 11 (1) (2021) 6224.
- [9] F. Ibrahim, A.L.I. Jaber, G. Ibrahim, E. Cheble, Antioxidant activity and total phenol content of different plant parts of Lebanese *Annona squamosa* Linn, *Int. J. Pharm. Pharm. Sci.* 12 (8) (2020) 100–105.
- [10] D.O.D. Leite, C.J. Camilo, C.d.F.A. Nonato, N.K.G.d. Carvalho, G.J.T. Salazar, S.M. de Moraes, J.G.M.d. Costa, Chemical profile and evaluation of the antioxidant and anti-acetylcholinesterase activities of *Annona squamosa* L. (Annonaceae) extracts, *Foods* 10 (10) (2021) 2343.
- [11] A. Rojas-Garcia, L. Rodriguez, M.L. Cadiz-Gurrea, A. Garcia-Villegas, E. Fuentes, M.D.C. Villegas-Aguilar, I. Palomo, D. Arraez-Roman, A. Segura-Carretero, Determination of the bioactive effect of custard apple by-products by in vitro assays, *Int. J. Mol. Sci.* 23 (16) (2022) 9238.
- [12] Y. Chen, Y. Chen, Y. Shi, C. Ma, X. Wang, Y. Li, Y. Miao, J. Chen, X. Li, Antitumor activity of *Annona squamosa* seed oil, *J. Ethnopharmacology* 193 (2016) 362–367.
- [13] D.M. El-Baz, A. Hssan, Effects of Egyptian *Annona squamosa* leaves extracts against alloxan induced hyperglycemia in rats, *World J. Pharm. Pharm. Sci.* (2019) 145–163.
- [14] Y. Wang, Y. Xiang, V.W. Xin, X.W. Wang, X.C. Peng, X.Q. Liu, D. Wang, N. Li, J.T. Cheng, Y.N. Lv, S.Z. Cui, Z. Ma, Q. Zhang, H.W. Xin, Dendritic cell biology and its role in tumor immunotherapy, *J. Hematol. Oncol.* 13 (1) (2020) 107.
- [15] M.K. Kim, J. Kim, Properties of immature and mature dendritic cells: phenotype, morphology, phagocytosis, and migration, *RSC Adv* 9 (20) (2019) 11230–11238.
- [16] W. Zhang, S.Y. Cho, G. Xiang, K.J. Min, Q. Yu, J.O. Jin, Ginseng berry extract promotes maturation of mouse dendritic cells, *PLoS One* 10 (6) (2015), e0130926.

- [17] P. Chauv, N. Favre, M. Martin, F. Martin, Tumor-infiltrating dendritic cells are defective in their antigen-presenting function and inducible B7 expression in rats, *Int. J. Cancer* 72 (4) (1997) 619–624.
- [18] S. Tsujitani, A. Kakeji Y Fau – Watanabe, S. Watanabe A Fau – Kohnoe, Y. Kohnoe S Fau – Maehara, K. Maehara Y Fau-Sugimachi, K. Sugimachi, Infiltration of dendritic cells in relation to tumor invasion and lymph node metastasis in human gastric cancer, *Cancer* 16 (1990) 2012–2016.
- [19] W.F.T. Carson, S.E. Salter-Green, M.M. Scola, A. Joshi, K.A. Gallagher, S.L. Kunkel, Enhancement of macrophage inflammatory responses by CCL2 is correlated with increased miR-9 expression and downregulation of the ERK1/2 phosphatase Dusp6, *Cell. Immunol.* 314 (2017) 63–72.
- [20] E.A. Speakman, I.M. Dambuza, F. Salazar, G.D. Brown, T cell antifungal immunity and the role of C-type lectin receptors, *Trends Immunol* 41 (1) (2020) 61–76.
- [21] J.L. Guerrier, Macrophages: Their untold story in T cell activation and function, *Int. Rev. Cel. Mol. Bio.* 342 (2019) 73–93.
- [22] B. Eiz-Vesper, H.M. Schmetszer, Antigen-presenting cells: potential of proven und new players in immune therapies, *Transfus. Med. Hemoth.* 47 (6) (2020) 429–431.
- [23] M. Yin, Y. Zhang, H. Li, Advances in research on immunoregulation of macrophages by plant polysaccharides, *Front. Immunol.* 10 (2019) 145.
- [24] S. Yu, R. Ma, X. Dong, H. Ji, A. Liu, A novel polysaccharide from *Boletus edulis*: Extraction, purification, characterization and immunologic activity, *Ind. Crops Prod.* 186 (2022), 115206.
- [25] Z. Liu, Z. Liu, L. Li, J. Zhang, Q. Zhao, N. Lin, W. Zhong, M. Jiang, Immunomodulatory effects of the polysaccharide from *Sinonovacula constricta* on RAW264. 7 macrophage cells, *Food Sci Nutr* 10 (2022) 1093–1102.
- [26] S.J. Kim, S.-H. Baek, K.S. Kang, M.-S. Shin, Characterization of macrophage activation after treatment with polysaccharides from ginseng according to heat processing, *Appl. Biol. Chem.* 66 (2023) 15.
- [27] L. Stich, S. Plattner, G. McDougall, C. Austin, A. Steinkasserer, Polysaccharides from european black elderberry extract enhance dendritic cell mediated T cell immune responses, *Int. J. Mol. Sci.* 23 (2022) 3949.
- [28] W. Tu, J. Zhu, S. Bi, D. Chen, L. Song, L. Wang, J. Zi, R. Yu, Isolation, characterization and bioactivities of a new polysaccharide from *Annona squamosa* and its sulfated derivative, *Carbohydr. Polym.* 152 (2016) 287–296.
- [29] Q. Ren, J. Chen, Y. Ding, J. Cheng, S. Yang, Z. Ding, Q. Dai, Z. Ding, In vitro antioxidant and immunostimulating activities of polysaccharides from *Ginkgo biloba* leaves, *Int. J. Biol. Macromol.* 124 (2019) 972–980.
- [30] Y. Fan, M. Lin, Q. He, M. Wang, A. Luo, Immunomodulatory activity of an acidic polysaccharide isolated from arrowhead, *J. Sci. Innovat. Res.* 3 (1) (2014) 81–84.
- [31] G. Xie, I.A. Schepetkin, M.T. Quinn, Immunomodulatory activity of acidic polysaccharides isolated from *Tanacetum vulgare L.*, *Int. Immunopharmacol.* 7 (13) (2007) 1639–1650.
- [32] Y. Jing, J. Zhu, T. Liu, S. Bi, X. Hu, Z. Chen, L. Song, W. Lv, R. Yu, Structural characterization and biological activities of a novel polysaccharide from cultured *Cordyceps militaris* and its sulfated derivative, *J. Agr. Food Chem.* 63 (13) (2015) 3464–3471.
- [33] C. Qin, K. Huang, H. Xu, Isolation and characterization of a novel polysaccharide from the mucus of the loach, *Misgurnus anguillicaudatus*, *Carbohydr. Polym.* 49 (3) (2002) 367–371.
- [34] W. Cai, L. Xie, Y. Chen, H. Zhang, Purification, characterization and anticoagulant activity of the polysaccharides from green tea, *Carbohydr. Polym.* 92 (2) (2013) 1086–1090.
- [35] A. Li Lin, N. Shangari, T.S. Chan, D. Ramirez, P.J. O'Brien, Herbal monoterpene alcohols inhibit propofol metabolism and prolong anesthesia time, *Life Sci* 79 (1) (2006) 21–29.
- [36] R. Yu, W. Yang, L. Song, C. Yan, Z. Zhang, Y. Zhao, Structural characterization and antioxidant activity of a polysaccharide from the fruiting bodies of cultured *Cordyceps militaris*, *Carbohydr. Polym.* 70 (4) (2007) 430–436.
- [37] A. Linker, L.R. Evans, G. Impallomeni, The structure of a polysaccharide from infectious strains of *Burkholderia cepacia*, *Carbohydr. Res.* 335 (1) (2001) 45–54.
- [38] B. Yang, Y. Jiang, M. Zhao, F. Chen, R. Wang, Y. Chen, D. Zhang, Structural characterisation of polysaccharides purified from longan (*Dimocarpus longan Lour.*) fruit pericarp, *Food Chem* 115 (2) (2009) 609–614.
- [39] K. Inaba, M. Inaba, N. Romani, H. Aya, M. Deguchi, S. Ikehara, S. Muramatsu, R.M. Steinman, Generation of large numbers of dendritic cells from mouse bone marrow cultures supplemented with granulocyte/macrophage colony-stimulating factor, *J. Exp. Med.* 176 (6) (1992) 1693–1702.
- [40] M.B. Lutz, N. Kukutsch, A.L. Ogilvie, S. Röbner, F. Koch, N. Romani, G. Schuler, An advanced culture method for generating large quantities of highly pure dendritic cells from mouse bone marrow, *J. Immunol. Methods* 223 (1) (1999) 77–92.
- [41] D. Qiao, J. Liu, C. Ke, Y. Sun, H. Ye, X. Zeng, Structural characterization of polysaccharides from *Hyriopsis cumingii*, *Carbohydr. Polym.* 82 (4) (2010) 1184–1190.
- [42] M.M.S. Asker, B.T. Shawky, Structural characterization and antioxidant activity of an extracellular polysaccharide isolated from *Brevibacterium otitidis* BTS 44, *Food Chem* 123 (2) (2010) 315–320.
- [43] H.S. Xu, Y.W. Wu, S.F. Xu, H.X. Sun, F.Y. Chen, L. Yao, Antitumor and immunomodulatory activity of polysaccharides from the roots of *Actinidia eriantha*, *J. Ethnopharmacol.* 125 (2) (2009) 310–317.
- [44] Z.Y. Zhu, N. Liu, C.L. Si, Y. Liu, L.N. Ding, C. Jing, A.J. Liu, Y.M. Zhang, Structure and anti-tumor activity of a high-molecular-weight polysaccharide from cultured mycelium of *Cordyceps gunnii*, *Carbohydr. Polym.* 88 (3) (2012) 1072–1076.
- [45] X. Pu, X. Ma, L. Liu, J. Ren, H. Li, X. Li, S. Yu, W. Zhang, W. Fan, Structural characterization and antioxidant activity in vitro of polysaccharides from *angelica* and *astragalus*, *Carbohydr. Polym.* 137 (2016) 154–164.
- [46] S. Li, C. Pan, W. Xia, W. Zhang, S. Wu, Structural characterization of the polysaccharide moiety of an aqueous glycopeptide from mannate, *Int. J. Biol. Macromol.* 67 (2014) 351–359.
- [47] M.M. Zhang, G. Wang, F.R. Lai, H. Wu, Structural characterization and immunomodulatory activity of a novel polysaccharide from *Lepidium meyenii*, *J. Agr. Food Chem.* 64 (9) (2016) 1921–1931.
- [48] W.Z. Liao, Z. Luo, D. Liu, Z.X. Ning, J.G. Yang, J.Y. Ren, Structure characterization of a novel polysaccharide from Dictyophora indusiata and its macrophage immunomodulatory activities, *J. Agric. Food Chem.* 63 (2) (2015) 535–544.
- [49] Y. Tao, J. Ma, C. Huang, C. Lai, Z. Ling, Q. Yong, The immunomodulatory activity of degradation products of *Sesbania cannabina* galactomannan with different molecular weights, *Int. J. Biol. Macromol.* 205 (2022) 530–538.
- [50] C. Liao, I. Lai, H. Kuo, S. Chuang, H. Lee, J. Whang-Peng, C. Yao, G. Lai, Epigenetic modification and differentiation induction of malignant glioma cells by oligo-fucoidan, *Mar Drugs* 17 (9) (2019) 525–528.
- [51] C. Li, Z. Dong, B. Zhang, Q. Huang, G. Liu, X. Fu, Structural characterization and immune enhancement activity of a novel polysaccharide from *Moringa oleifera* leaves, *Carbohydr. Polym.* 234 (2020), 115897.
- [52] H. Li, J. Li, H. Shi, C. Li, W. Huang, M. Zhang, Y. Luo, L. Song, R. Yu, J. Zhu, Structural characterization and immunoregulatory activity of a novel acidic polysaccharide from *Scapharca subcrenata*, *Int. J. Biol. Macromol.* 210 (2022) 439–454.
- [53] A.M. Stern, J. Zhu, An introduction to nitric oxide sensing and response in bacteria, *Adv. Appl. Microbiol.* 87 (2014) 187–220.
- [54] Q. Xue, Y. Yan, R. Zhang, H. Xiong, Regulation of iNOS on immune cells and its role in diseases, *Int. J. Mol. Sci.* 19 (12) (2018) 3805.
- [55] M. Zhao, J. Hou, S. Zheng, X. Ma, X. Fu, S. Hu, K. Zhao, W. Xu, *Peucedanum praeruptorum* Dunn polysaccharides regulate macrophage inflammatory response through TLR2/TLR4-mediated MAPK and NF-kappaB pathways, *Biomed. Pharmacother.* 152 (2022), 113258.
- [56] X. Zhang, C. Qi, Y. Guo, W. Zhou, Y. Zhang, Toll-like receptor 4-related immunostimulatory polysaccharides: Primary structure, activity relationships, and possible interaction models, *Carbohydr. Polym.* 149 (2016) 186–206.
- [57] D. Peng, Y. Wen, S. Bi, C. Huang, J. Yang, Z. Guo, W. Huang, J. Zhu, R. Yu, L. Song, A new GlcNAc-containing polysaccharide from *Morchella importuna* fruiting bodies: Structural characterization and immunomodulatory activities *in vitro* and *in vivo*, *Int. J. Biol. Macromol.* 192 (2021) 1134–1149.